J Mater Sci: Mater Electron (2016) 27:33–39
DOI 10.1007/s10854-015-3713-9

Ferromagnetism in Fe-doped MgO nanoparticles

Sumalin Phokha[1] · **Jutharatana Klinkaewnarong**[1] · **Sitchai Hunpratub**[1] ·
Kornkanok Boonserm[2] · **Ekaphan Swatsitang**[3] · **Santi Maensiri**[4]

Received: 28 May 2015 / Accepted: 28 August 2015 / Published online: 4 September 2015

Abstract This work reports the study on magnetic properties of $Mg_{1-x}Fe_xO$ (x = 0, 0.05 and 0.07) nanoparticles prepared by the polymer pyrolysis method. Phase, valence states and magnetic properties of these samples were characterized using X-ray diffraction (XRD), transmission electron microscopy, X-ray absorption near edge structure (XANES) and vibrating sample magnetometer (VSM), respectively. The XRD results show that the samples have a phase nature of the cubic structure with constant crystallite size of 25 ± 2 nm. XANES spectra reveal the existence of Fe^{3+} ions in the samples. VSM measurements exhibit the room temperature ferromagnetism with a maximum magnetization of 1.60 emu/g for x = 0.07. The origin of ferromagnetism is fitted on the bound magnetic polaron (BMP) model to indicate the numbers of BMPs involving overlapping of polarons via oxygen vacancy defects.

1 Introduction

Oxide-based dilute magnetic semiconductors (O-DMSs) and insulator oxides which can exhibit a ferromagnetic (FM) with Curie temperature (T_c) above room temperature (RT), have attracted much due to its potential application in spintronic devices [1, 2]. These O-DMSs and insulating such as ZnO, TiO_2, SnO_2, In_2O_3, CeO_2, CaO or MgO display RT-FM with just a few percent of a transition-metal (TM) doping such as V, Cr, Mn, Fe, Co or Ni when grown as thin film [3–6] or in powder form [7, 8], etc. Several models of RT-FM have been proposed for these semiconductors and insulators, including a new exchange mechanism involving donor electrons in an impurity, the carrier (electron) mediated exchange mechanism and F-center exchange (FCE) as on defect mediated mechanism, especially oxygen vacancies (V_O) [7, 9, 10]. Some experimental and theoretical results report that the V_O plays an important role in the magnetic origin for wide band gap oxides/insulators [11]. However, this is still not well understood and a unified framework capable of explaining this is needed.

Magnesium oxide (MgO) is an insulator with a wide band gap of 7.8 eV and exhibit diamagnetism in bulk form. Early work on MgO based was focused on nanocrystalline form due to the capability in the magnetic property improvement. For example, the RT-FM can be observed in nanocrystalline MgO with particle size of ∼10–50 nm [11–14]. The authors suggested that this behavior was attributed to the Mg vacancy defect at the surface of the nanoparticles. Recently, Maoz et al. [15] also found RT-FM in MgO nanosheet, which originated from V_O. This suggested that the RT-FM in this sample could be necessarily induced by Mg vacancy and/or V_O based on FCE. Further, the substitution on Mg ions by various transition metal such as $Mg_{1-x}Fe_xO$ [16], $Mg_{1-x}Ni_xO$ [17],

---

✉ Sumalin Phokha
sumalinphokha@gmail.com

[1] Department of Physics, Faculty of Science, Udon Thani Rajabhat University, Udon Thani 41000, Thailand

[2] Department of Applied Chemistry, Faculty of Science and Liberal Arts, Rajamangala University of Technology Isan, Nakhon Ratchasima 30000, Thailand

[3] Integrated Nanotechnology Research Center and Department of Physics, Faculty of Science, Khon Kaen University, Khon Kaen 40002, Thailand

[4] School of Physics, Institute of Science, Suranaree University of Technology, Nakhon Ratchasima 30000, Thailand

$Mg_{1-x}Mn_xO$ [18] and $Mg_{1-x}Cr_xO$ [19] can improve the magnetic properties. Therefore, it is of great interest to study the magnetic properties in nanocrystalline $Mg_{1-x}Fe_xO$ powders as promising ferromagnetic materials for the understanding of future spintronic devices.

In this work, we report the magnetic properties of Fe-doped MgO ($Mg_{1-x}Fe_xO$, x = 0, 0.05 and 0.07) nanoparticles prepared by the polymer pyrolysis method. The crystallinity, morphology, and valence states of $Mg_{1-x}Fe_xO$ samples were characterized by X-ray diffraction (XRD), transmission electron microscopy (TEM) and X-ray absorption near edge spectroscopy (XANES). The magnetic properties of $Mg_{1-x}Fe_xO$ samples were investigated using a vibrating sample magnetometer (VSM).

2 Experimental

Nanoparticles of Fe-doped MgO ($Mg_{1-x}Fe_xO$, x = 0, 0.05 and 0.07) were synthesized by the polymer pyrolysis method according to our previous work [20]. 0.006 mol of $Mg(NO_3)_2{\cdot}6H_2O$ (Aldrich), $Fe(NO_3)_3{\cdot}9H_2O$ (Kanto) and 70 ml of acrylic acid ($C_3H_4O_2$) were dissolved in deionized water to promote the polymerization. The precursor solution was stirred and heated at 30 °C until it dried. Then the final product was pre-calcined in a furnace at 400 °C for 2 h to form the polyacrylate salt. The precursor was then calcined at a temperature of 700 °C for 3 h in air to obtain the cubic phase of MgO.

The prepared samples were characterized using XRD, XANES and VSM. Bruker D2 Phaser X-ray diffractometer with Cu Kα radiation ($\lambda = 0.154184$ nm) was used to study the phases of the $Mg_{1-x}Fe_xO$ samples. The morphology and crystal structure of the samples were performed using TEM (TEM Ziess, EM902, Germany). XANES spectra of Fe *K* edges were studied using X-ray absorption near edge spectroscopy in transmission mode at the BL5.2 line at Siam Photon (Synchrotron Research Institute) in Nakhon Ratchasima, Thailand. The magnetic measurements were performed at room and low temperature using a vibrating sample magnetometer (Versa Lab VSM, Quantum Design) in the field cooling (FC) mode with an applied field of 500 Oe.

3 Results and discussion

Figure 1 shows the XRD patterns of $Mg_{1-x}Fe_xO$ nanoparticles with x = 0, 0.05 and 0.07. All samples exhibit peaks consistent with the cubic structure of MgO in the standard JCPDS 78-0430 and the diffraction peak corresponding to the impurity phase of Fe_3O_4 is observed in sample of x = 0.07. It also shows that Fe ions might have been substituted into the MgO lattice due to no impurity phase of Fe_3O_4 in the sample of x = 0.05. The Rietveld analysis confirms the cubic structure [space group Fm-3m (225)] of all samples, as shown in Fig. 2. The average crystallite sizes (*D*) of all samples were calculated from the X-ray line broadening using Scherrer's equation. The crystallite size of 25 ± 2 nm is remained with

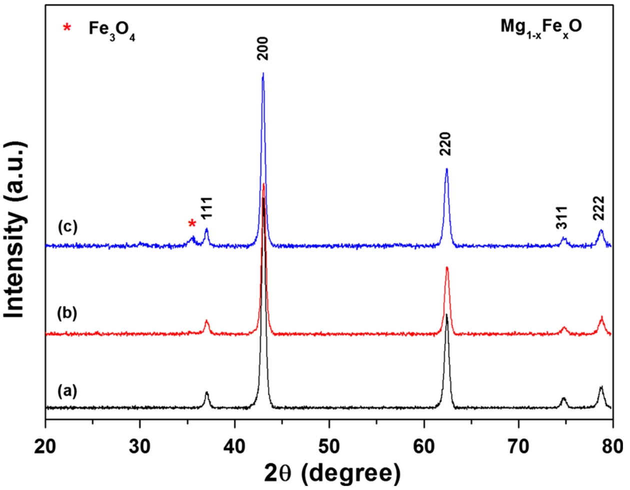

Fig. 1 XRD patterns of $Mg_{1-x}Fe_xO$ nanoparticle calcined at 700 °C for samples with *a* x = 0, *b* x = 0.05 and *c* x = 0.07

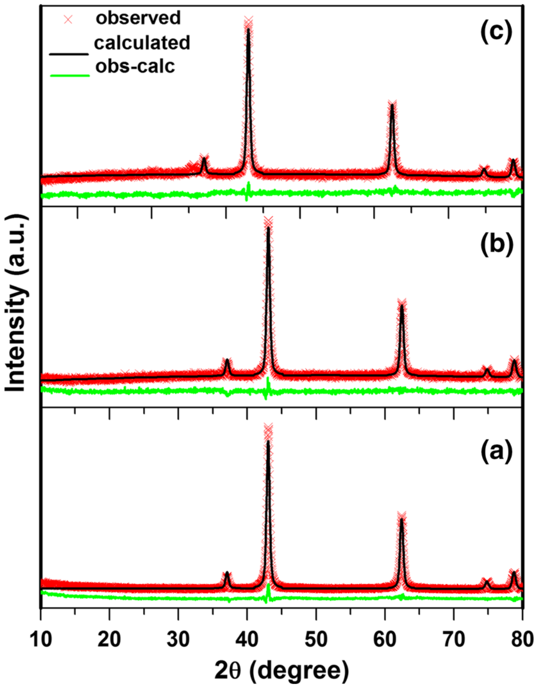

Fig. 2 Refined X-ray diffraction patterns of $Mg_{1-x}Fe_xO$ nanoparticle calcined at 700 °C for samples with **a** x = 0, **b** x = 0.05 and **c** x = 0.07. The experimental data are indicated by the *dots* and the calculated data by the *solid line* overlaying them; the *bottom curve* shows the difference between the experimental and calculated data

increasing Fe content (as listed in Table 1). The effect of Fe doping on the lattice parameter (*a*) as obtained from the Rietveld analysis is observed to be decreased from 0.4217(4) to 0.4213(4) nm with increasing Fe content, as shown in Table 1. This is possibly due to the replacement of the larger Mg^{2+} ions (0.89 Å) by the smaller Fe^{3+} ions (0.78 Å). This causes a change in the Mg–O bond length (lattice distortion) and the overall lattice parameter, which is in good agreement with earlier reports [18, 21].

The morphology and structure of $Mg_{1-x}Fe_xO$ nanoparticles are investigated by TEM with the selected area electron diffraction (SAED) patterns, as shown in Fig. 3. TEM bright field images show aggregated nanoparticles. The average particle size of the samples was evaluated from the histogram in the inset of Fig. 3 to be 25 ± 1 nm, which is consistent with the XRD results. It can be also seen from the inset in Fig. 3 that a single particle of the samples is in the range of 24–26 nm. The SAED patterns of the samples showed the spotty ring patterns suggesting a formation of polycrystalline structure. This also agrees well with the XRD results.

The valence states of Fe in $Mg_{1-x}Fe_xO$ samples are obtained from the XANES measurements. The XANES spectra at Fe K-edge were measured at room temperature. Figure 4 shows edge energies of the Fe foil, FeO (Fe^{2+}) standard, Fe_3O_4 (Fe^{2+}, Fe^{3+}) standard, Fe_2O_3 (Fe^{3+}) standard, and $Mg_{1-x}Fe_xO$ samples with (a) $x = 0.05$ (b) $x = 0.07$. The structure of shift of the edge position can be used to determine the valence state of Fe in the $Mg_{1-x}Fe_xO$ samples. From Fig. 3, the edge position of FeO (Fe^{2+}) standard is approximately 7120 eV, while that of Fe_3O_4 (Fe^{2+}, Fe^{3+}) standard is approximately 7122 eV. In addition, edge position of Fe_2O_3 (Fe^{3+}) standard is approximately 7124 eV. These can be simply used as a fingerprint of phases and valence states. It is seen that the edge positions of all samples are quite similar to that of the Fe^{3+} standard, indicating the Fe^{3+} valence state for most of the Fe ions in all samples.

Figure 5a shows the magnetic field dependence of the specific magnetization (*M*–*H* curve) obtained from VSM measurements for MgO nanoparticles measured from 50 to 300 K (room temperature, RT) with magnetic field (*H*) in the range of ±30 kOe. Each sample exhibits ferromagnetism (FM) component with large hysteresis loop and diamagnetic increased at higher *H*. Therefore, the magnetization (*M*) is subtracted in terms of the Eq. (1):

$$M = M_f + \chi_p H \tag{1}$$

where χ_p is the slope at high *H* and then saturated magnetization (M_S) from subtraction is $M_f = M - \chi_p H$ [22]. The inset shows the subtraction of MgO sample measured at 300 K with the M_S value of 0.035 emu/g (as summarized in Table 1). The sample shows well FM and largest hysteresis loop measured at 50 K as shown in Fig. 5b. The M_S value decreases with increasing measuring temperature, due to the thermal fluctuations causing the randomization of polarization direction. However, the slight decrease of M_S measured at 300 K compared to that measured at 50 K can contribute to the Curie temperature (T_C) above 300 K. This observed T_C corresponds to the obtained result from field cooling (FC) curve, as shown in the Fig. 7. This observed ferromagnetism in this MgO nanoparticle is of great interest because bulk MgO is diamagnetic ordering [23]. Based on previous analysis of FM component in MgO nanoparticles, it is suggested that this FM behavior results from the vacancy defects [e.g., oxygen vacancies (V_O) and/or Mg vacancies (V_{Mg})] at the surfaces of the nano-crystals [18, 24, 25]. The M_s value of 0.035 emu/g (~25 nm in size) of our MgO nanoparticles is much higher than that of 0.0026 emu/g for MgO nanoparticles (~11.9 nm) synthesized by precipitation method [18] and the value of 0.025 emu/g for MgO nanoparticles (~20 nm) synthesized by co-precipitation method [24]. The difference in the *M* value of MgO materials depends on the preparation conditions as originated from vacancy defects at the surface of nanoparticles. This behavior has been also observed in other oxides as well as in ZnO [26–28], TiO_2 [29], and CeO_2 [30]. Therefore, for ferromagnetism in oxides, the defects are also the important effect.

The *M*–*H* curves obtained from VSM measurements at RT for $Mg_{1-x}Fe_xO$ nanoparticles with *H* in the range of ±30 kOe are shown in Fig. 6. All samples show well FM

Table 1 Summary of crystallite sizes (*D*) estimated from XRD line broadening, lattice parameter (*a*) calculated from Rietveld refined XRD patterns, magnetization (*M*) at RT, and fitting parameters extracted from BMP model of $Mg_{1-x}Fe_xO$ nanoparticles calcined in air at 700 °C for 3 h

Samples $Mg_{1-x}Fe_xO$	*D* (nm)	Rietveld refinement		*M* (emu/g)	Fitting parameters		
		a (nm)	χ^2		M_o (emu/g)	$N \times 10^{16}$ (cm^{-3})	$\chi_m \times 10^{-5}$ (egs)
x = 0	25.7 ± 2.6	0.4217 (4)	1.34	0.035	–	–	–
x = 0.05	25.5 ± 2.0	0.4215 (4)	0.85	0.14	0.08	0.093	0.43
x = 0.07	25.5 ± 2.5	0.4213 (4)	1.23	1.60	1.26	1.32	1.6

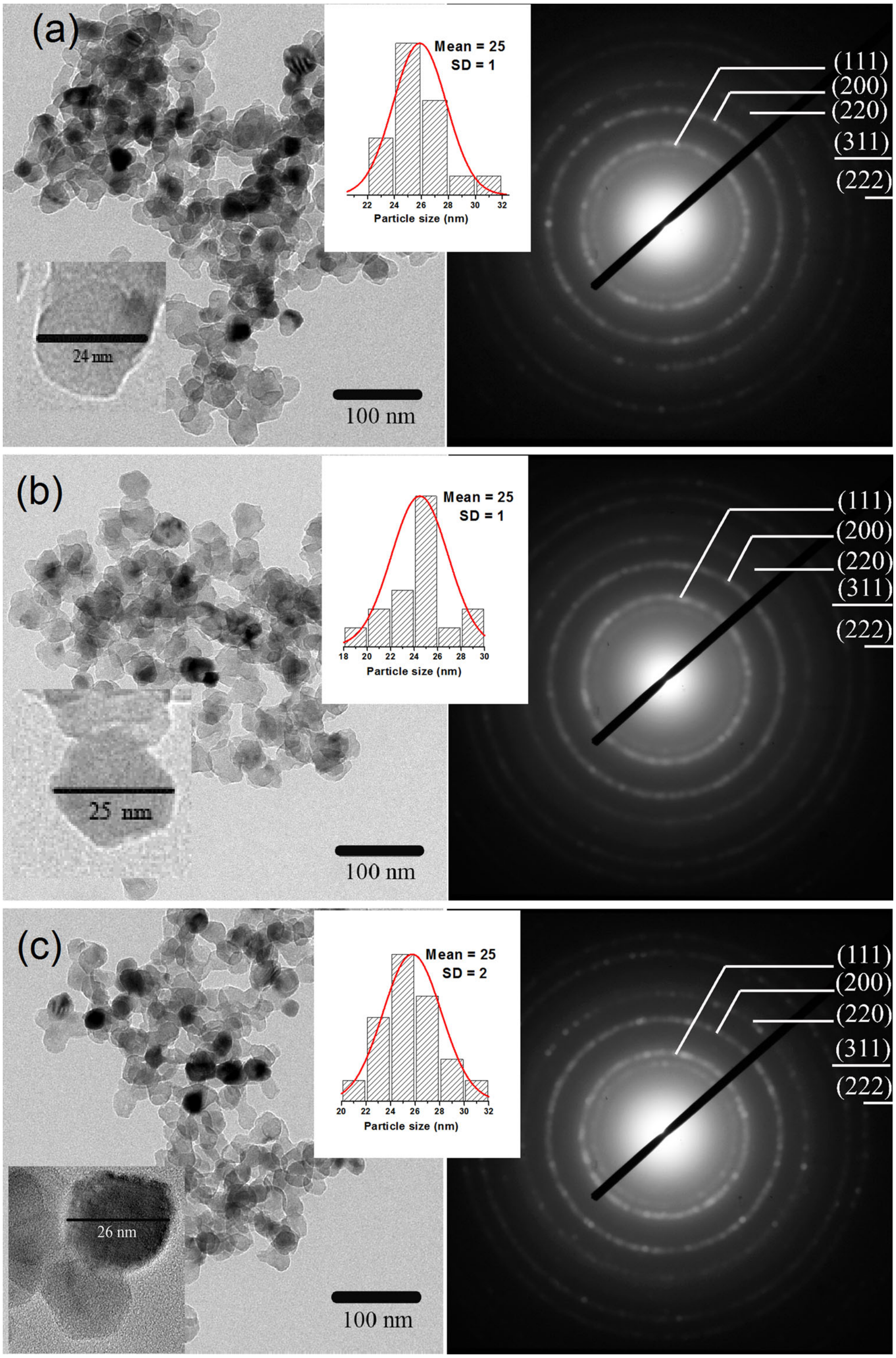

Fig. 3 TEM images with selected-area electron diffraction (SAED) patterns of $Mg_{1-x}Fe_xO$ nanoparticle calcined at 700 °C for samples with **a** $x = 0$, **b** $x = 0.05$ and **c** $x = 0.07$. *Inset* shows the histogram and a single particle of the samples

with increasing of M_s from 0.14 to 1.60 emu/g due to the increase of Fe content, as summarized in Table 1. The Fe substitution causes a decrease of the coercive field (H_c) compared to that of the pure MgO nanoparticle. This RT-FM behavior in our $Mg_{1-x}Fe_xO$ nanoparticles can be explained by the existence of oxygen vacancies (V_O) based on bound magnetic polarons (BMP). The VO is naturally formed to ensure charge neutrality, which is sensitive to any disorder in the oxygen sublattice resulting from thermal, doping and/or substitution technique and preparation conditions (e.g., high temperature heating in vacuum or different atmospheres or ion-bombarding of the surface)

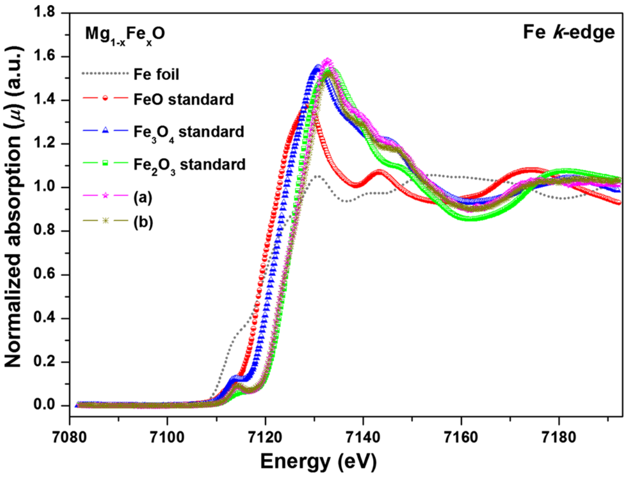

Fig. 4 XANES spectra at the Fe K absorption edge of the Fe foil, FeO (Fe^{2+}) standard, Fe_3O_4 (Fe^{2+}, Fe^{3+}) standard, Fe_2O_3 (Fe^{3+}) standard and $Mg_{1-x}Fe_xO$ nanoparticles calcined at 700 °C for samples with *a* x = 0.05 and *b* x = 0.07

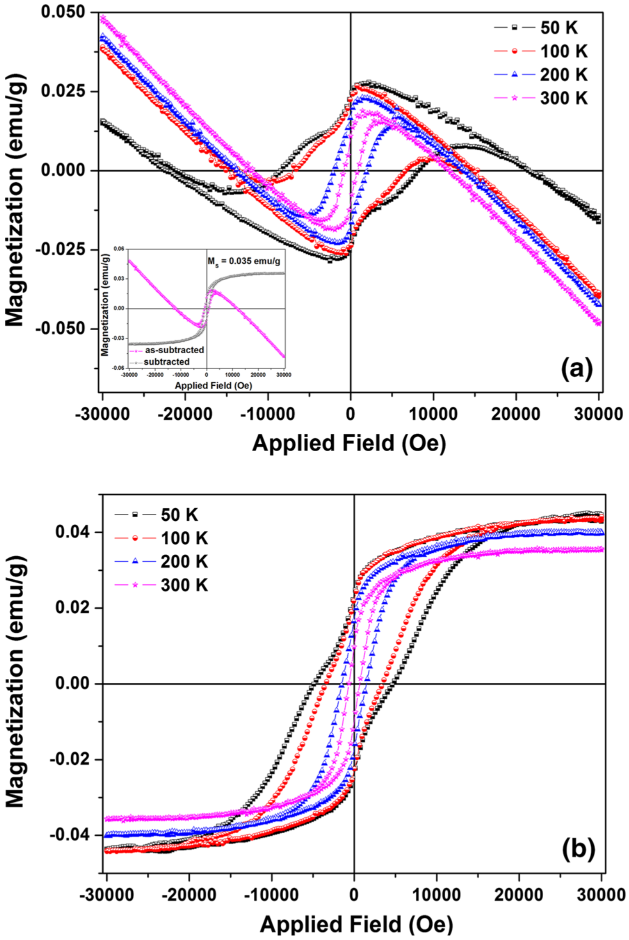

Fig. 5 *M–H* curves for MgO nanoparticles measured at various temperatures **a** ferromagnetism with diamagnetic component and **b** the obtained M_s after subtraction of diamagnetic component for all temperatures. *Inset* of (**a**) shows the different *M–H* curves measured at room temperature

[31]. According to the BMP model, the large density of VO results more BMPs and neighboring BMPs can overlap in the long-range FM coupling. To consider the number of BMPs, the *M–H* curves can be well fitted using a simple BMPs model Eq. (2) [32]:

$$M = M_0 L(x) + \chi_m H \qquad (2)$$

where the first term is from BMP contribution and the second term is due to paramagnetic matrix contribution. $M_0 = Nm_s$, N is the number of BMPs involved and m_s is the effective spontaneous moment per BMP. $L(x) = \coth(x) - 1/x$ is the Langevin function with $x = m_{eff} H/(k_B T)$, where m_{eff} is the true spontaneous moment per BMP, and at higher temperature it can be approximated to $m_s = m_{eff}$. The values of the parameters M_0, N and χ_m of the samples are listed in Table 1. The *M–H* curves fitted with BMP model for Fe-doped MgO samples are plotted in the insets of Fig. 6, which exhibit a good fit for each sample. The parameters are found to increase with increasing of Fe content to be from 0.08 to 1.26 emu/g, 9.3×10^{14} to 1.32×10^{16} cm^{-3} and 4.3×10^{-6} to 1.6×10^{-5} egs for M_0, N and χ_m, respectively. The number of BMPs in our samples is close to that of Ni-doped ZnO nanoparticles ($N = 10^{15}$ cm^{-3}) [32] and Co-doped ZnO nanoparticles ($N = 10^{17}$ cm^{-3}) [33], which is required for a long-range FM order. However, the difference in the number of BMPs depends on the availability of free carriers of various materials. Thus, the RT-FM in our results can be explained by V_O interaction based on the BMP model.

Figure 7 shows the temperature dependence of magnetization (*M–T* curve) for the samples with x = 0 and 0.05 measured under the *H* of 500 Oe between 50 and 400 K in the FC mode. Both samples show similar behavior of FC curve and no evidence of secondary phase can be detected. The T_C of samples can be determined from the derivative of the magnetization of $dM_{FC}(T)/dT = 0$ [34]. In this case, the result of the magnetization curve shows that the T_C of both samples is above 400 K. Thus, it is necessary to design FM oxide materials with high T_C above RT and high thermal equilibrium stability during the device fabrication process.

4 Conclusion

$Mg_{1-x}Fe_xO$ nanoparticles with the crystallite sizes of approximately 25 ± 2 nm have been prepared by the polymer pyrolysis method. Structural characterization showed the cubic phase of MgO and detected the impurity phase of Fe_3O_4 with sample of x = 0.07. Bright field TEM images showed the agglomeration of nanoparticles with size of 25 ± 1 nm, corresponding to the stable size

Fig. 6 *M–H* curves for $Mg_{1-x}Fe_xO$ nanoparticles measured at room temperature for samples with *a* x = 0.05 and *b* x = 0.07. *Insets* show the fitting BMP model for samples with *a* x = 0.05 (*lower*) and *b* x = 0.07 (*upper*)

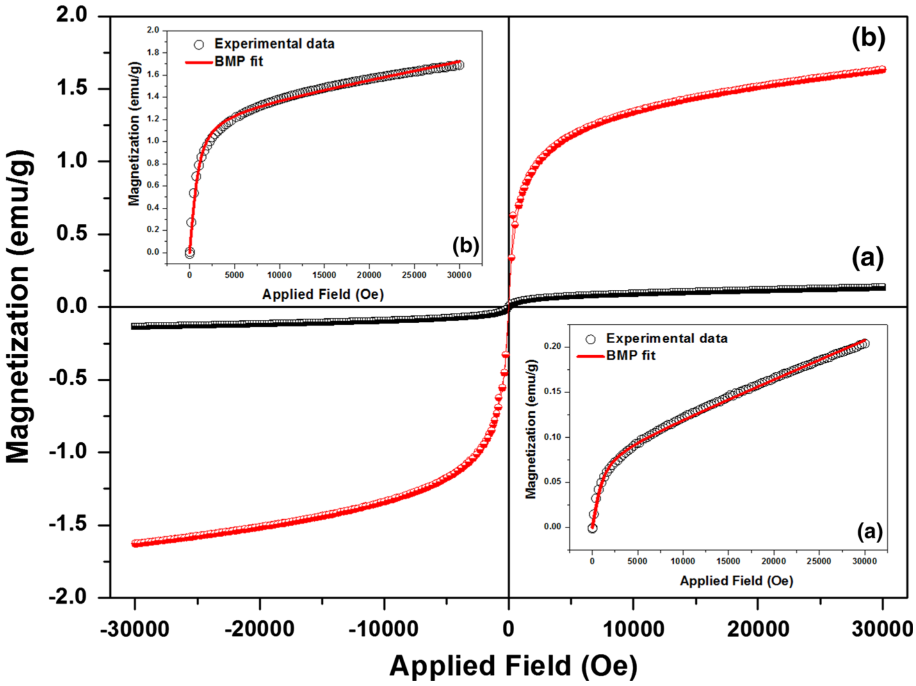

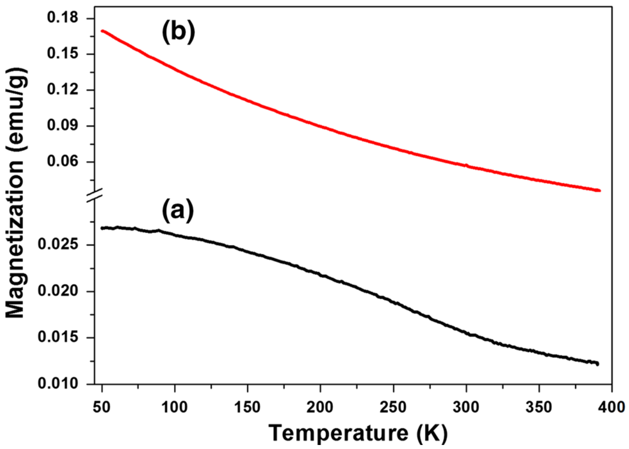

Fig. 7 *M–T* curves at 500 Oe of $Mg_{1-x}Fe_xO$ nanoparticles for samples with *a* x = 0 (*lower*) and *b* x = 0.05 (*upper*)

obtained from the XRD results. The valence state of Fe^{3+} ions were observed in the $Mg_{1-x}Fe_xO$ nanoparticles and higher concentration doping of Fe^{3+} caused of as high as the defects/oxygen vacancy. This oxygen vacancy induced ferromagnetic behavior at room temperature in $Mg_{1-x}Fe_xO$ nanoparticles based on BMP model. Additionally, the high T_C of nanoparticles was observed above 400 K. It is suggested that the stable room temperature ferromagnetism in $Mg_{1-x}Fe_xO$ nanoparticles can potentially be useful for the future spintronics and transparent nanodevices.

Acknowledgments The authors would like to thank the Synchrotron Light Research Institute (Public Organization), Nakhon Ratchasima, Thailand for XANES facilities, the Department of Physics, Khon Kaen University for providing VSM facilities and the Advanced Materials Physics (AMPs) Laboratory for our research.

References

1. T. Dietl, H. Ohno, F. Matsukura, J. Cibert, D. Ferrand, Science **287**, 1019 (2000)
2. S.J. Pearton, W.H. Heo, M. Ivill, D.P. Norton, T. Steiner, Semicond. Sci. Technol. **19**, R59 (2004)
3. J.M.D. Coey, Curr. Opin. Solid State Mater. **10**, 83 (2006)
4. N.H. Hong, J. Sakai, W. Prellier, A. Hassini, A. Ruyter, F. Gervais, Phys. Rev. B **70**, 195204 (2004)
5. C.B. Fitzgerald, M. Venkatesan, L.S. Dorneles, R. Gunning, P. Stamenov, J.M.D. Coey et al., Phys. Rev. B **74**, 115307 (2006)
6. A. Tiwari, V.M. Bhosle, S. Ramachandran, N. Sudhakar, J. Narayan, S. Budak, A. Gupta, Appl. Phys. Lett. **88**, 142511 (2006)
7. J. Philip, A. Punnoose, B.I. Kim, K.M. Reddy, S. Layne, J.O. Holmes, B. Satpati, P.R. LeClair, T.S. Santos, J.S. Moodera, Nat. Mater. **5**, 298 (2006)
8. S. Phokha, S. Pinitsoontorn, S. Maensiri, J. Appl. Phys. **112**, 113904 (2012)
9. J.M.D. Coey, M. Venkateshan, C.B. Fitzgerald, Nat. Mater. **4**, 173 (2005)
10. Q.Y. Wen, H.Y. Zhang, Q.H. Yang, Y.Q. Song, J.Q. Xiao, J. Magn. Magn. Mater. **321**, 3110 (2009)
11. J.F. Hu, Z.L. Zhang, M. Zhao, H.W. Qin, M.H. Jiang, Appl. Phys. Lett. **93**, 192503 (2008)
12. M. Sterrer, E. Fischbach, T. Risse, H.J. Freund, Phys. Rev. Lett. **94**, 186101 (2005)
13. N. Kumar, D. Sanyal, A. Sundaresan, Chem. Phys. Lett. **477**, 360 (2009)
14. D.D. Wang, Z.Q. Chen, C.Y. Li, X.F. Li, C.Y. Cao, Z. Tang, Phys. B **407**, 2665 (2012)

15. B.M. Maoz, E. Tirosh, M. Bar Sadan, G. Markovich, Phys. Rev. B **83**, 161 (2011)
16. A. Shalimov, K. Potzger, D. Geiger, H. Lichte, G. Talut, A. Misiuk, H. Reuther, F. Stromberg, S. Zhou, C. Baehtz, J. Fassbender, J. Appl. Phys. **105**, 064906 (2009)
17. S. Ramachandran, J. Narayan, J.T. Prater, Appl. Phys. Lett. **90**, 132511 (2007)
18. S. Azzaza, M. El-Hilo, S. Narayanan, J.J. Vijaya, N. Mamouni, A. Benyoussef, A. El Kenz, M. Bououdina, Mater. Chem. Phys. **143**, 1500 (2014)
19. F. Stavale, N. Nilius, H.J. Freund, New J. Phys. **14**, 033006 (2012)
20. S. Phokha, S. Hunpratup, S. Pinitsoontorn, B. Putasaeng, S. Rujirawat, S. Maensiri, Mater. Res. Bull. **67**, 118 (2015)
21. S. Suwanboon, P. Amornpitoksuk, A. Sukolrat, Ceram. Int. **37**, 1359 (2011)
22. M.S. Seehra, S. Suri, V. Singh, J. Appl. Phys. **111**, 07B516 (2012)
23. G. Sharma, P. Jeevanandam, Microporous Mesoporous Mater. **165**, 55 (2013)
24. ChN Rao, U.T. Nakate, R.J. Choudhary, S.N. Kale, Appl. Phys. Lett. **103**, 151107 (2013)
25. B. Choudhury, A. Choudhury, Mater. Res. Express **1**, 025026 (2014)
26. A.N. Andriotis, R.M. Sheetz, M. Menon, J. Phys. Condens. Matter **22**, 334210 (2010)
27. G.Z. Xing, Y.H. Lu, Y.F. Tian, J.B. Yi, C.C. Lim, Y.F. Li, G.P. Li, D.D. Wang, B. Yao, J. Ding, Y.P. Feng, T. Wu, AIP Adv. **1**, 022152 (2011)
28. X. Bie, C. Wang, H. Ehrenberg, Y. Wei, G. Chen, X. Meng, G. Zou, F. Du, Solid State Sci. **12**, 1364 (2010)
29. S.D. Yoon, Y. Chen, A. Yang, T.L. Goodrich, X. Zuo, D.A. Arena et al., J. Phys. Condens. Matter **18**, L355 (2006)
30. S. Phokha, S. Pinitsoontorn, P. Chirawatkul, Y. Poo-arporn, S. Maensiri, Nanoscale Res. Lett. **7**, 425 (2010)
31. I. Kosacki, T. Suzuki, V. Petrovsky, H.U. Anderson, P. Colomban, Solid State Ion. **149**, 99 (2002)
32. G. Srinet, R. Kumar, V. Sajal, J. Appl. Phys. **114**, 033912 (2013)
33. B. Pal, P.K. Giri, J. Nanosci. Nanotechnol. **11**, 1 (2011)
34. X. Zhou, J. Xue, D. Zhou, Z. Wang, Y. Bai, X. Wu, X. Liu, J. Meng, ACS Appl. Mater. Interf. **2**, 2689 (2010)